3D Pneumatic & 2D Dynamic Probes: Their Development and Subsequent Use in a Transonic Fan

M.A. Cherrett, J.D. Bryce
DRA Farnborough, UK

H.P. Hodson
Cambridge University, UK

SUMMARY

Three different 3D pneumatic probes have been built and calibrated in detail, along with two dynamic yawmeters and a geometrically identical pneumatic yawmeter. This paper discusses the aerodynamic performance of the probes and compares detailed steady-state flowfield measurements taken with the probes at stator exit in a transonic fan.

1 INTRODUCTION

Aerodynamics & Propulsion Department at DRA-Pyestock is engaged in a programme to study the viscous endwall and blade wake flows in high-speed compressors and fans. As part of this programme an extensive series of tests has been carried out to measure, in detail, the flowfield within a single stage transonic fan known as C148. A large amount of specialised instrumentation was developed for this purpose, including; a) several 3D pneumatic traverse probes, b) 2D dynamic yawmeter traverse probes, c) instrumented stator blades containing high-response pressure transducers and thin-film gauges (which are not discussed in this paper).

The 3D pneumatic and the dynamic yawmeter probes were calibrated in detail at the Whittle Laboratory in order to determine their aerodynamic characteristics. This paper discusses these characteristics and also compares time-averaged stator exit flowfield measurements taken with the different probes in C148.

2 PROBES

2.1 3D Pneumatic Probes

Fig 1 shows the 3 pneumatic probe designs used. Probe A is a 4-hole wedge probe design similar to that described by Heneka[1] and Bubeck & Wachter[2]. The triangular cross section of the probe has a 25° included angle and an axial chord of 5.5mm. This cross section is maintained for 25mm before blending into the circular cross section of the support stem. The bottom of the probe is inclined downward by 20° to the horizontal and is provided with a pressure tapping to facilitate pitch angle measurement.

The sensing head of probes B & C is a truncated 3-sided pyramid similar to the probe design reported by Shepherd[3]. Probe B is a stem mounted probe, as is probe A, while probe C is a sting mounted probe where the measuring plane is 41mm upstream of the probe support stem centre line. Two versions of probe C were manufactured, one with a horizontal sting and one inclined downward by 15° to match the C148 annulus geometry and hence allow measurements to be taken in the stator hub region. Only the inclined probe is reported in this paper.

The sensing head of probe B was machined from solid while probe C was constructed by bonding hypodermic tubes to a machined core and grinding the tube ends to form the pyramid shape. The dimensions of both pyramid probe heads were the same, with the three static pressure ports positioned on a pitch circle diameter of 3.0mm. The axes of the static tappings were all forward facing rather than perpendicular to the pyramid faces. Probe B has a shielded thermocouple mounted above the pyramidal head of the probe for stagnation temperature measurements.

An important consideration when designing the 3D pneumatic probes was that they should be relevant to future dynamic probe development. Hence 4-hole, rather than 5-hole, designs were selected in order to avoid taking redundant pressure measurements. This is an important consideration for dynamic probes where the data capture and processing overheads, associated with dynamic pressure measurements, are high. Further, while smaller probes could have been built, this would not have been consistent with probe geometries capable of housing four unsteady pressure transducers (using methods such as those developed at Oxford University[4] for on-blade transducer mounting).

2.2 Dynamic Yawmeter

Fig 2 shows the dynamic yawmeter probe which was developed at Rolls-Royce plc with joint UK MoD/DTI/Rolls-Royce funding. The triangular cross section of the probe has an included angle of 30° and an axial chord of 5.6mm. Three semiconductor pressure transducers are contained within the sensing head of the probe. The transducer for measuring stagnation pressure is a Kulite type XCQ-062, while the two static pressure transducers are Kulite type LQ-047. All transducers had a range of 344kPa absolute and were coated with a 0.05-0.08mm layer of silastomer rubber for protection. The two static pressure transducer diaphragms lay flush with the probe surface. Two identical yawmeters were used in C148. In addition a pneumatic version of the dynamic yawmeter design was also calibrated at the Whittle Laboratory. A more detailed account of the design and development of the dynamic

yawmeters is given by Cook[5].

Compensation for semiconductor pressure transducer temperature sensitivity was achieved using a system developed at DRA which has been reported by Cherrett & Bryce[6]. A schematic diagram of the system is shown in Fig 3. A thermally stable 'sense' resistor is placed in series with the transducer excitation circuit. As the transducer bridge resistance changes with temperature, the current drawn by the transducer strain gauge bridge changes. This induces a change in the dc voltage across the 'sense' resistor. Hence, if the transducer is calibrated over a range of pressures at a series of constant temperatures, the change in voltage across the 'sense' resistor can be correlated with transducer diaphragm temperature. Therefore, when used to take measurements, the 'sense' voltage can be used to determine the transducer diaphragm temperature. This then allows calculation of the correct transducer pressure sensitivity and null pressure offset to allow conversion of the transducer pressure output to absolute pressure.

The DRA yawmeter transducers were subjected to repeated calibrations over a period spanning one year, including the period when the yawmeters were used in the C148 test programme. This allowed the transducer null pressure offset drift to be characterized. This indicated that, over the period when the yawmeters were used in C148, transducer absolute pressure measurement accuracy was 0.35% of full scale deflection. This degree of pressure measurement uncertainty corresponds to an absolute yaw angle measurement uncertainty of ±0.5° at Mach 0.85, and ±1.5° at Mach 0.5. However, ad hoc comparisons of the transducer outputs with barometric pressure, during the C148 test series, allowed the degree of measurement uncertainty to be reduced. Further work is in progress to quantify the performance attained, and hence the amount of yaw angle, stagnation pressure and static pressure uncertainty associated with the dynamic yawmeter measurements.

3 PROBE AERODYNAMIC CALIBRATIONS

3.1 Calibration Facility

All of the 3D probes and the dynamic yawmeters were calibrated using the Transonic Cascade Test Facility at the Whittle Laboratory (Dominy & Hodson[7]). This is a closed circuit , variable density wind tunnel in which Mach number and Reynolds number can be varied independently at ambient temperature. The test section was fitted with a transonic nozzle similar to that developed by Baines[8] in which the upper and lower walls were perforated to provide continuous acceleration over a range of subsonic and supersonic exit Mach numbers without changing nozzle geometry. The stagnation pressure was measured in the upstream plenum and the static pressure variation through the nozzle was determined from a set of pressure tappings at mid-height along one of the side walls. Confirmation that these static pressure measurements were representative of those across the nozzle was found by comparing needle static probe measurements with static pressure data derived from Schlieren photographs.

Tunnel and probe pressures were measured using a single transducer by means of a Scanivalve arrangement. Absolute pressure measurement was estimated to be accurate to ±0.1kPa and relative pressure measurement to ±0.04kPa. The probes were positioned at the centre of the nozzle exit plane by a computer controlled traverse system. Probe pitch and yaw angles could be adjusted in steps of 0.02° with an absolute accuracy better than 0.2°.

The nozzle measures 0.08m x 0.10m. Hence, for the stem mounted probes (probe A, probe B and the dynamic yawmeter) blockage accounted for approximately 3.0% of the nozzle exit area. Stem probe blockage was estimated from the projected frontal area of the probes. Sting probe blockage was thought to be negligible as the probe support stem was positioned at a distance greater than 7 probe stem diameters downstream of the nozzle exit plane.

3.2 3D Probe Calibrations

Data from the 3D probe calibrations were processed to yield five coefficients: the yaw coefficient (C_{YAW}), the pitch coefficient (C_{PIT}), the probe pressure ratio coefficient (C_{PR}), the stagnation pressure coefficient (C_{STAG}), and the static pressure coefficient (C_{STAT}). Where:

$$C_{yaw} = \frac{(S2-S3)}{(P1-P_{mean})}$$

$$C_{pit} = \frac{(S4-S_{2+3}) \ . \ k}{(P1-P_{mean})}$$

$$C_{pr} = \frac{P_{mean}}{P1}$$

$$C_{stag} = \frac{(P1-Po)}{(P1-P_{mean})}$$

$$C_{stat} = \frac{(Po-p)}{(P1-P_{mean})}$$

where:

$$S_{2+3} = \frac{S2+S3}{2} \qquad P_{mean} = \frac{Sa+Sb}{2}$$

i) P1,S2,S3 & S4 are the probe pressure port readings as defined in Fig 1.

ii) Sa,Sb,Sc are S2,S3,S4 sorted into ascending order.

iii) k=1 for probe A and -1 for probes B & C, ie, to allow for the pitch port being above the yaw port plane for probe A and below the yaw plane for probes B & C.

iv) Po & p are the calibration tunnel stagnation & static pressures.

C_{YAW}, C_{PIT}, and C_{PR} form primary coefficients which are combined to form a 3D calibration space within a processing algorithm. When presented with experimental data, ie, measured values of C_{YAW}, C_{PIT}, and C_{PR}, the processing algorithm searches the calibration space to yield corresponding values of yaw angle, pitch angle and estimated Mach number (via the probe pressure ratio coefficient). Stagnation and static pressures are then derived from C_{STAG} and C_{STAT} and the correct value of Mach number is then calculated.

The stem probes were calibrated over a yaw angle range of ±30° and a pitch angle range of -5° to +30°. The sting probe was calibrated over a yaw angle range of ±26° and a pitch angle range of -50° to +20°. All of the probes were calibrated at a Reynolds number of $55x10^3$. The characteristic length used to define Reynolds number was taken as the axial chord length (of 5.5mm) for probe A, while the sensing head diameter (of 3.5mm) was used for the pyramid probes. This was consistent with C148 stator exit conditions at mid-span for the pyramid probes. However, the 4-hole wedge probe should have been calibrated at a Reynolds number of $89x10^3$ to be consistent with C148 stator exit conditions.

A pyramid probe similar to probes B & C was calibrated at Reynolds numbers of $5.5x10^3$ and $55x10^3$. Reynolds number effects were found to be negligible. Reynolds number effects were not investigated specifically for the 4-hole wedge probe (A). However, calibration of the dynamic and pneumatic yawmeter probes (see section 3.3) at Reynolds numbers of $36x10^3$ and $90x10^3$ did not reveal any significant effects. Further, Dominy & Hodson[7], found little Reynolds number dependency above $40x10^3$ for 5-hole conical and pyramid probes. Hence the failure to calibrate the 4-hole probe at a high enough Reynolds number, compared to those found at C148 stator exit, was not expected to introduce any significant errors into measurements taken with this probe.

The aerodynamic characteristics of the three 3D probes are illustrated in Figs 4,5 & 6. Fig 4 shows the relationship between C_{YAW} and C_{PIT}. The data are illustrated by lines of constant yaw angle and pitch angle. Only data at one Mach number are shown because similar behaviour was seen at other Mach numbers. It is evident that the 4-hole wedge probe (A) is far less sensitive to yaw and pitch angle than the pyramid probes. Further, C_{YAW} and C_{PIT} for probe A are strongly dependant on both yaw and pitch angle while the pyramid probes display this characteristic to a far smaller extent.

The C_{PR} data, shown in Fig 5, indicate the number of Mach numbers at which the probes were calibrated. Probe C, the sting pyramid probe, was calibrated most extensively because it was expected to yield the best measurements due to its low blockage. Both of the other probes could have benefited from more extensive Mach number calibration to minimise linearisation errors associated with the processing algorithm. The C_{PR} data are observed to become more dependant on yaw and pitch angle with increasing Mach number. However, none of the C_{PR} planes penetrate each other, which would result in conditions that would cause failure of the interpolative processing algorithm.

Fig 6 shows C_{PIT}, for each probe, plotted against pitch angle where the individual lines represent C_{PIT} variation with pitch angle at a constant yaw angle. Fig 6 indicates a notable 15° downwash effect on probe B. Probe A displays more complex behaviour, with variable degrees of stem downwash experienced at yaw angles greater than ±10°. This is somewhat surprising as maintaining the wedge cross section for a considerable distance away from the probe sensing head was intended to minimise such effects. Further work is required to explain more fully the flow about the probe head and stem causing this behaviour.

3.3 Dynamic Yawmeter Calibration

Data from the yawmeter calibration were processed to yield three coefficients that are subsequently used by an iterative algorithm to solve for the required flow parameters. The coefficients consist of the yaw coefficient (C_{YAWR}), the stagnation pressure coefficient (C_{STAGN}), and the static pressure coefficient (C_{STATIC}). These, and a further coefficient, C_{RMS}, which characterizes the static transducer pressure unsteadiness, are plotted in Fig 7 for one of the DRA dynamic yawmeters. Where:

$$C_{yawr} = \frac{(S2-S3)}{(P_o-p)}$$

$$C_{stagn} = \frac{(P1-P_o)}{(P_o-p)}$$

$$C_{static} = \left(\frac{(P_o-p)}{p}\right) \times \left(\frac{S_m}{(P1-S_m)}\right)$$

$$C_{skrms} = \frac{\sqrt{s_k^2}}{(P_o-p)}\Big|_{k=2,3}$$

where: s_2 & s_3 are the time average of the unsteady static tapping pressure signals.

$$S_m = \frac{(S2+S3)}{2}$$

The form of these coefficients differ from those used for the 3D pneumatic probes primarily to satisfy the requirements of the iterative processing algorithm. However, the C_{STATIC} coefficient is more complex than the corresponding 3D probe version in an attempt to derive a less Mach number dependant parameter. This is illustrated in Fig 7, where apart from at Mach 0.9 C_{STATIC} is insensitive to Mach number. Further, C_{YAWR} is also insensitive to Mach number, as is C_{STAGN} in the yaw angle range -10° to +10°. The C_{STAGN} data at Mach 0.3 are displaced from the C_{STAGN} data at higher Mach numbers. This is an artefact of transducer measurement uncertainty and the small dynamic head (15 kPa) associated with satisfying the Mach number and Reynolds number conditions in the wind tunnel.

C_{RMS} behaviour gives an insight into the quasi-steady flow about the probe. Firstly, it is evident that the non-dimensionalised unsteadiness associated with the flow about the probe decreases with Mach number. Further, it is noted that at yaw angles less than -10° and greater than +10° the leeward transducer outputs display increasing levels of unsteadiness as the flow about the probe begins to separate. Note that at positive yaw angles transducer S3 is the leeward transducer, while S2 is the leeward transducer at negative yaw angles. At yaw angles less than -25° and greater than +25° the flow becomes fully separated and the transducer unsteadiness levels decrease markedly. Examination of C_{YAWR} behaviour reveals that this behaviour is manifest as changes in the coefficient slope.

One of the two DRA dynamic yawmeters, and a pneumatic version of the yawmeter design, were calibrated at Reynolds numbers of $36x10^3$ and $90x10^3$. This did not reveal any significant Reynolds number sensitivity. In addition, calibrations were carried out at pitch angles of -5°,+5°,10° and 15°, over the ±45° yaw angle range, for the dynamic yawmeter and at pitch

angles of -5°,0°,+5°,10° and 15°, at zero yaw, for the pneumatic yawmeter. Data resulting from calibration of the dynamic yawmeter at Mach 0.9 are shown in Fig 8. The effect of pitch angle on C_{YAWR} and C_{STAGN} behaviour is small for the pitch settings of +5°,+10° & +15°. However, negative pitch does introduce greater changes in the coefficient behaviour. Examination of the pneumatic yawmeter pitch calibration, although not illustrated here, shows that characteristics between 0° and 15° remain relatively constant. It is only when introducing flow at negative pitch to the probe that the characteristics change markedly. Further, it is noted that C_{STAGN} reaches a maximum value at approximately +10° of pitch indicating a stem downwash effect. Pitch angle effects have not been taken into account in the processing algorithm, and further work is required to quantify their influence.

4 TRANSONIC FAN MEASUREMENTS

The C148 single stage fan rig delivers a design pressure ratio of just over 1.8 at a flow of 53.3 kg/s. It has an un-snubbered rotor that operates with a tip speed of 444 m/s and a tip relative Mach number of 1.5. The rig is shown schematically in Fig 9. Overall fan pressure and temperature rise are measured at a plane approximately two axial stator chords downstream of the stator trailing edge using six pneumatic Pitot rakes and six shielded Keil thermocouple rakes equi-spaced about the annulus. Radial and circumferential traversing is available at two planes downstream of the stator trailing edge (at 36% and 118% axial stator chord downstream). Only measurements taken at the 36% downstream plane are discussed in this paper. Pneumatic static pressure tappings are provided in the hub and casing endwalls at each traverse plane. A more detailed description of C148 and its performance is given by Bryce et al[9].

The compressor performance characteristic is shown in Fig 10. This was measured at the beginning of the C148 test series during which 350 hours of rig running were accumulated. This paper will concentrate on measurements taken at peak efficiency operation on the design speed characteristic. Unfortunately, the measurements taken with each of the probes were not consecutive, and large numbers of rig running hours were accumulated between each of the measurements. (The sting pyramid probe (C) measurements were taken after 112 hours while the 4-hole wedge probe (A), stem pyramid probe (B), and dynamic yawmeter probe measurements were taken after 189, 249 & 294 hours respectively).

During the C148 test series the performance was noted to change for the same rig throttle setting. Further work is required to quantify the extent to which this change was due to mechanical wear, the accumulation of dirt on the blading, or the accumulation of dirt on the rig instrumentation (even though the rig was cleaned mid way through the test series). In addition the chronological characteristics of the change have yet to be fully investigated. The fan performance achieved during each of the traverse probe measurements is shown in Fig 10 using different symbols which indicate the degree of fan performance change during the test series.

Overall area averaged stagnation pressure ratio measurements, taken with the fixed downstream Pitot rakes, agreed to within 1.3% of that attained during the first traverse (when the sting pyramid probe was used). Similarly corrected mass flow agreed to within 1.0% of the sting pyramid traverse value. However, agreement between the Pitot rake measurements taken when the sting pyramid probe was used and when the 4-hole wedge probe was used was to within 0.12% pressure ratio. The corresponding mass flow measurements agreed to within 0.4%.

Fig 11 illustrates the salient features of the stator flowfield at design speed, peak efficiency, operation. Stagnation pressure measurements taken with each of the four probes are shown along with schematic illustrations of each probe at the correct scale relative to the annulus. The data have been normalized with respect to the fan exit rake stagnation pressure measurements, recorded during each run, in an attempt to suppress the effects of fan performance change. (That is, the data have been divided by the area averaged fan exit stagnation pressure and multiplied by the design pressure ratio of 1.807.) The sting pyramid probe (C) data consist of 16 radial by 38 circumferential measurements. The 4-hole wedge probe (A), dynamic yawmeter and stem pyramid probe (B) data consist of 21x38,10x20 & 10x20 measurements respectively. The measurements in the circumferential direction are equi-spaced. The dynamic yawmeter data have been derived from determining the time-averaged value at each traverse point from data phase-locked to a once per revolution signal and processed over 128 consecutive rotor revolutions. The duration of the time traces spanned the passing of 22 of the 25 rotor blade passages. Cherrett and Bryce[6] give a fuller description of this data capture and processing procedure.

It is clear from Fig 11 that a significant endwall corner separation is found at the hub. The associated high loss (low pressure) region is flanked by a high pressure region induced by the locally reduced passage area. Large velocity gradients and high unsteadiness levels are found in the shear layer bounding these two regions which makes accurate measurements particularly difficult. The stator wakes are observed to thicken with increasing span and there is also evidence of weaker endwall corner stall in the casing-suction surface region of the annulus.

The data shown in Fig 11 show encouraging qualitative agreement between each of the probe data sets although it is evident that stem pyramid probe (B) does not resolve the hub endwall corner separation region very well. In order to quantify agreement between the different probe data Fig 12 shows radial distributions of stagnation and static pressure ratio as well as yaw and pitch angles. These data have been determined by numerically averaging the data shown in Fig 11 in the circumferential direction over one stator pitch. Stagnation and static pressure data have been normalized relative to fan exit stagnation pressure. In addition, the static pressure ratio data have been shifted so that the casing endwall static pressure measurements, taken during each run, are superimposed.

The probe stagnation pressure measurements, shown in Fig 12a, agree to within ±0.5% of design stagnation pressure rise at mid-span. In order to determine to what extent the disagreement between the probe pressure measurements is due to probe geometry, or to fan performance changes, attention is drawn to Fig 12b. This shows the mean stagnation pressure ratio measurements recorded by the six Pitot rakes downstream of the stator. These data have also been normalized relative to the fan delivery stagnation pressure. The pressure profiles at this plane differs from those recorded at the traverse probe plane due to mixing of the flow. However, the degree of agreement between the Pitot rake measurements gives an indication of the fan performance related changes in the measurements, as the configuration of the rake measurements remained constant throughout the test series. The rake data are in better agreement than the probe measurements. In general, they agree to within ±0.2% of design pressure ratio at mid

span although the measurements associated with the sting pyramid probe and 4-hole wedge probe traverses agree to within ±0.08%.

The static pressure ratio measurements, taken with the traverse probes, are shown in Fig 12c. These agree to within ±3.1% of dynamic head at mid-span (note that the range of the pressure ratio axis in the static pressure plot is half that used in the stagnation pressure plot). The symbols at 0% and 100% span indicate the endwall static pressures measured by the pressure tappings.

It is evident that only the 4-hole wedge probe (A) data are in good agreement with the endwall measurements at both hub and casing. The sting pyramid probe (C) and 4-hole wedge probe (A) data agree well at mid-span although the sting pyramid probe indicates higher static pressures than recorded by the hub endwall tappings. Lower static pressures than measured on the casing endwall are recorded by the sting pyramid probe. The stem pyramid probe (B) indicates lower than expected static pressures over much of the span and behaves erratically toward the hub, where 3D viscous flows dominate. The dynamic yawmeter data agree reasonably well with the hub static pressure tapping measurements but are significantly higher than the values suggested from the casing static pressure tappings. Despite the qualitative variations in the static pressure distribution measured by the different probes, the quantitative agreement at mid-span is encouraging.

The yaw angle data, in Fig 12d, reveal that the sting pyramid probe (C) and 4-hole wedge probe (A) agree to within ±0.5° over much of the span and agree well with the design intent stator exit flow angle of -2.1° at mid-span. The dynamic yawmeter data are in good qualitative agreement with these measurements. However, they are shifted by +1° from the consensus achieved between the sting pyramid and 4-hole wedge measurements. The stem pyramid measurements show an even larger (+3° to +4°) difference.

In the case of the dynamic yawmeters, the sensing heads consist of cartridges that can be removed from their traverse stems. Indeed, the cartridges were not calibrated with their stems attached in the Whittle Laboratory tunnel. Hence it is possible that a mechanical alignment error may have been overlooked when setting up the probes in the wind tunnel, or on subsequent assembly of the cartridge and probe stem. Calibration and inspection records have yet to be re-evaluated. However, future analysis of other traverse measurements taken elsewhere on the fan performance characteristic will confirm whether this is a systematic alignment error or not. In addition the effect of the 1% mass flow change between the first two and last two traverses needs to be evaluated. However, it is not thought that this can account for the discrepancies observed in the stem pyramid measurements.

The pitch angle measurements taken with the sting pyramid probe (C) and 4-hole wedge probe (A), shown in Fig 12e, agree to within ±0.5° over much of the span. However, marked disagreement is noted in the hub endwall corner stall region. The stem pyramid probe data indicate pitch angles 2.5-3° higher than the other probes.

5 DISCUSSION

Clearly the stem pyramid probe (B) does not perform well in C148. This is thought to be a consequence of the effective pitch angle incident on the probe. This arises from the stem downwash (+15°), the geometry of the annulus (+14° at the hub and -2° at the casing) and the viscous flowfield.

The sting pyramid probe was expected to yield the most reliable measurements due to its low frontal blockage (compared with the stem probes) and alignment with the annulus geometry in the lower half of the annulus. In general the probe performed well, although the associated static pressure measurements were found to exhibit more endwall proximity influence than expected. Toward the casing, the probe alignment was not matched to the casing annulus wall geometry and hence may account for the recording of lower than expected static pressures in this region. However the reason for recording higher pressures toward the hub, than implied from the hub static pressure tappings, needs further investigation. It is suggested that, as the axial length of the probe is greater than the stem probes, the endwall profile is effectively modified locally. Hence, although the probe has a lower frontal blockage, when it lays near the endwall the interference between the probe and the endwall is larger than that experienced with the stem probes.

The performance of the 4-hole wedge probe was better than expected, given the probe's more complicated aerodynamic characteristics. Therefore, although the close agreement between static pressure measurements taken with this probe and the endwall static pressure tappings appear to suggest the probe performs better than the sting pyramid probe, acceptance of this conclusion is deferred until confirmation through analysing traverses taken at other fan operating points.

Agreement between the dynamic yawmeter and the consensus achieved between the sting pyramid and 4-hole wedge probes is adequate; given the more complex nature of the measurements, and that the probe being a 2D sensor in a highly 3D flowfield. It is suspected, although yet to be confirmed, that the discrepancy between the yaw angle measurements with this and the aforementioned pneumatic probes is caused largely by systematic mechanical alignment errors. If this proves not to be the case the result is more disappointing. However, it must be remembered that the dynamic yawmeter yields information on the unsteady flowfield (which has not been presented in this paper).

6 CONCLUSIONS

1) Three different 3D pneumatic probes (a 4-hole wedge probe, a stem pyramid probe, and a sting pyramid probe) have been built and carefully calibrated. The 4-hole wedge probe displayed the most complex behaviour, manifest as strong dependency on both yaw and pitch angle, of its calibration coefficients. All of the probes displayed negligible Reynolds number sensitivity for the Reynolds number range 5.5×10^3 to 55×10^3.

2) Two identical dynamic yawmeters, and a geometrically identical pneumatic yawmeter, have been built and calibrated in detail. The probes were not sensitive to Reynolds number variation in the range 36×10^3 to 90×10^3. Pitch angle sensitivity was found to be small in the range 0° to +15°, although -5° did produce more significant influence on the yawmeter coefficients.

3) The three 3D pneumatic probes and the dynamic yawmeters have been used to take detailed flow measurements in a single stage transonic fan. To date, detailed comparison has been carried out between measurements taken with these different probes at stator exit, while the fan was operating at peak efficiency at design speed. The sting pyramid probe and 4-hole wedge probes agreed with each other most closely. The dynamic yawmeter measurements showed adequate agreement with the consensus achieved by the aforementioned probes; while the stem pyramid

performance was disappointing.

4) Future work is required to address the following.

i) It is required to investigate the sting pyramid probe endwall interference characteristics, particularly with regard to their influence on static pressure measurement.

ii) It is necessary to confirm that the 4-hole wedge probe performs as well during traverses carried out at other fan operating points.

iv) It is necessary to confirm whether the dynamic yawmeter angle measurement uncertainty has arisen from mechanical alignment errors or otherwise.

5) Comparison of the different probe measurements underlines the need to understand the complex interaction between probe geometry, turbomachine geometry and the flowfield being measured. Intrusive measurements in high-speed turbomachinery are still an essential tool for improved design and computational fluid dynamics code validation. However, such measurements are often carried out with too little understanding of the above issues. Where possible, cross referencing with non-intrusive measurements should be carried out.

ACKNOWLEDGEMENTS

Dr O Jadayel made a significant contribution to much of the probe aerodynamic calibration work. Dr Jadayel now works at Birmingham University, UK. This work was supported by the UK Ministry of Defence and the Department of Trade & Industry.

REFERENCES

NO.	AUTHOR.	TITLE,etc.
1	A Heneka	Instantaneous three-dimensional four-hole wedge probe. Proc. of 7th Symposium on Measurement Techniques for Transonic & Supersonic Flows in Cascades & Turbomachines, Aachen (1983)
2	H Bubeck J Wachter	Development & application of a high frequency wedge probe. ASME 87-GT-216 (1987)
3	I C Shepherd	A four hole pressure probe for fluid flow measurements in three dimensions. ASME Journal of Fluids Engineering, Vol 103, pp.590-594, (1981)
4	R W Ainsworth, A J Dietz, T Nunn	The use of semiconductor sensors for blade surface pressure measurements in a model turbine stage. ASME 90 -GT-346 (1990)
5	S C Cook	Development and use of a high response aerodynamic wedge probe and its use on a high speed research compressor. Proc. of the Ninth International Symposium on Air Breathing Engines, Athens. Vol 1 pp.1113-1125, (1989)
6	M A Cherrett, J D Bryce	Unsteady viscous flow in a high speed core compressor. ASME 91-GT-91 (1991)
7	R G Dominy, H P Hodson	An investigation of factors influencing the calibration of 5-hole probes for 3D flow measurements. ASME 92-GT-216 (1992)
8	N C Baines	Development of a perforated nozzle for calibrating transonic probes. Proc. of 7th Symposium on Measurement Techniques for Transonic & Supersonic Flows in Cascades & Turbomachines, Aachen (1983)
9	J D Bryce, M A Cherrett, P A Lyes	Three-dimensional flow in a highly loaded single-stage transonic fan. ASME 93-GT (1993)

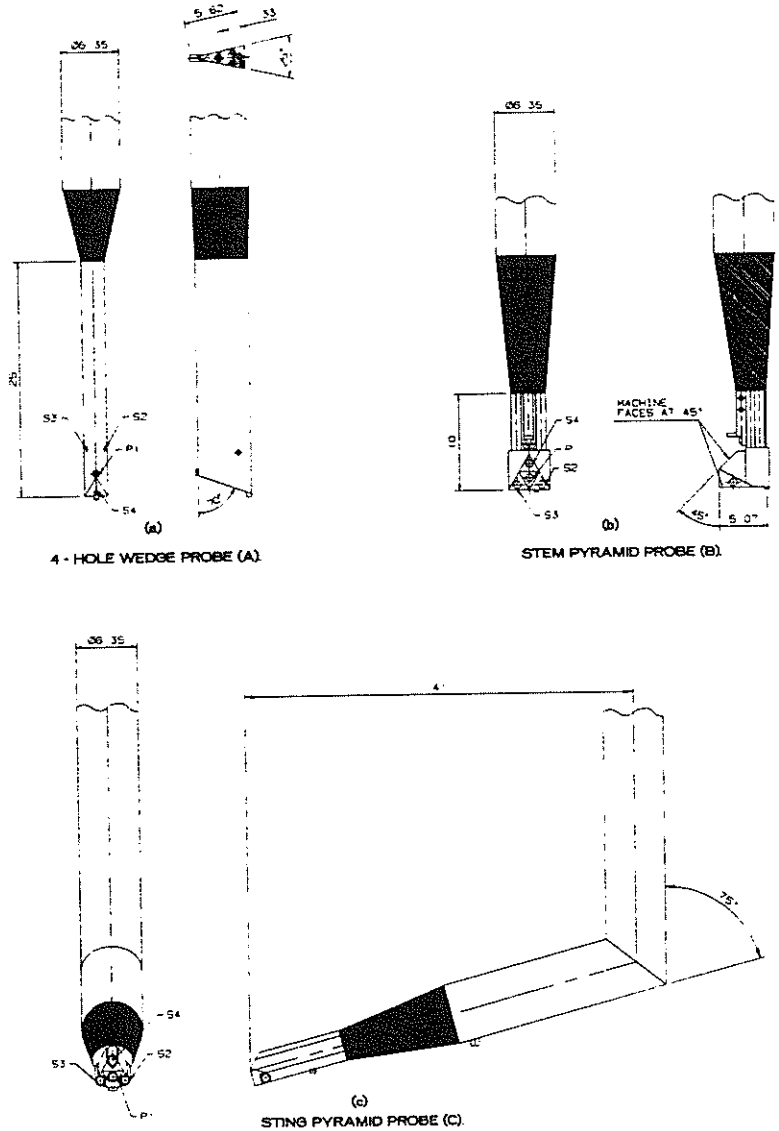

Fig 1: The three 3D pneumatic probes used.

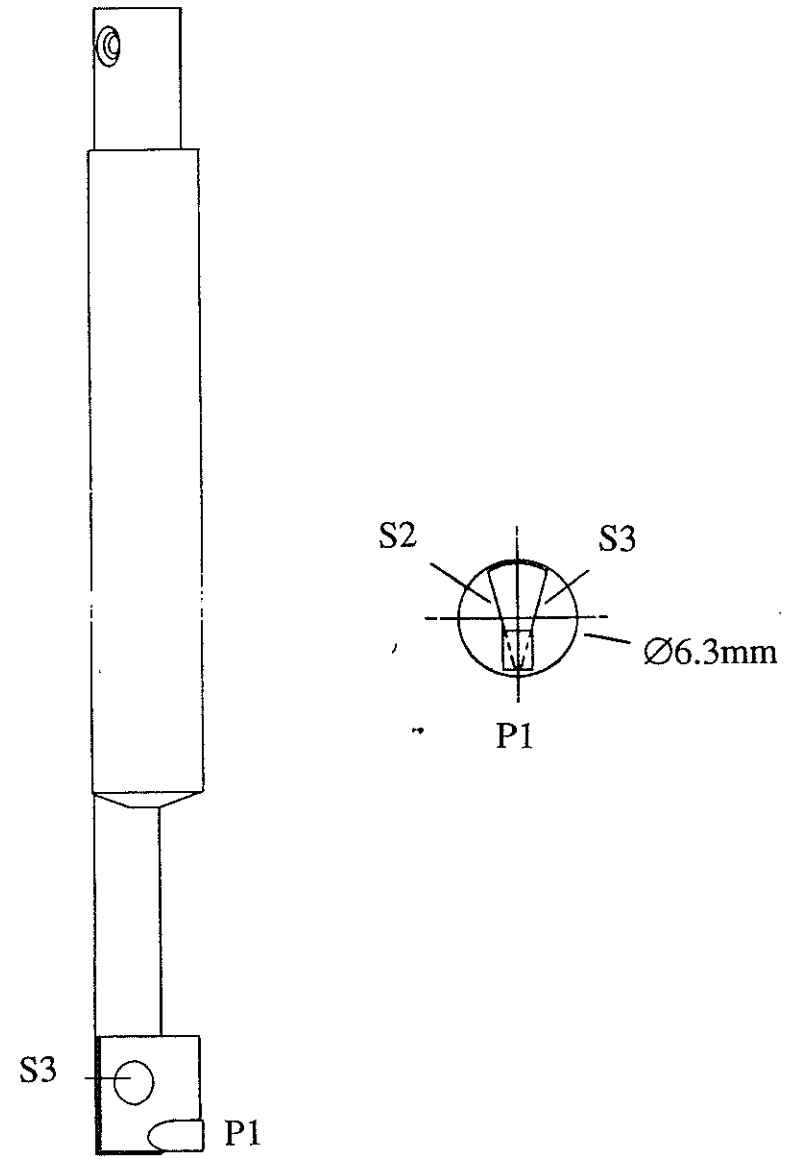

Fig 2: The dynamic yawmeter.

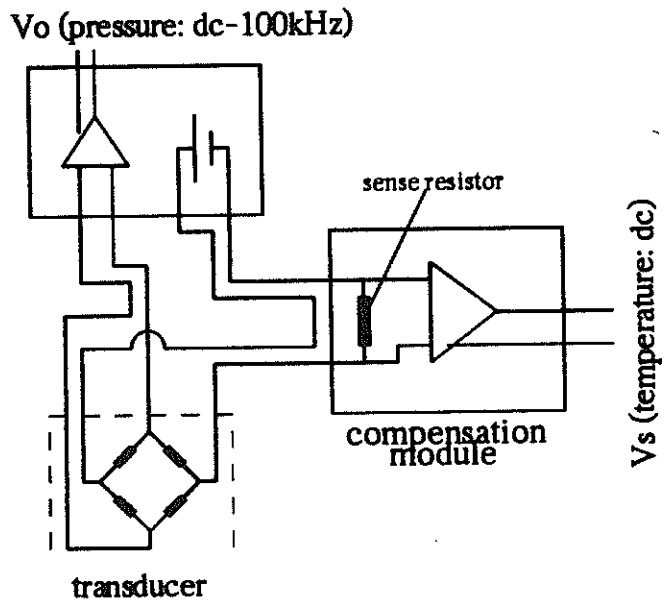

Fig 3: The DRA semiconductor pressure transducer thermal error compensation system.

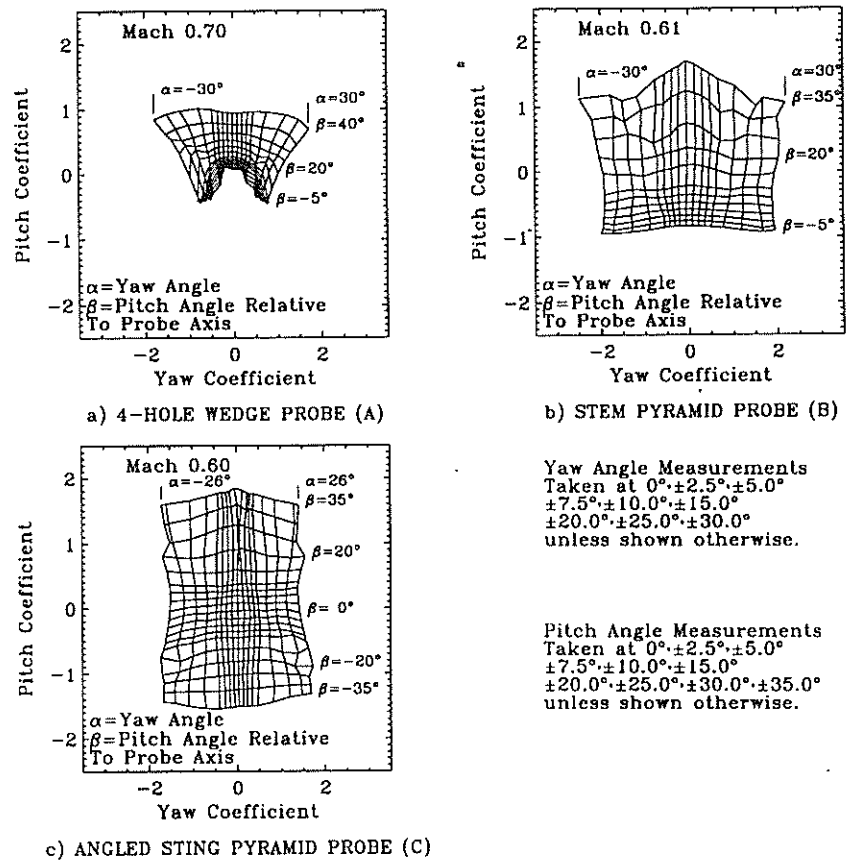

Fig 4: Yaw coefficient vs pitch coefficient behaviour for the 3D pneumatic probes.

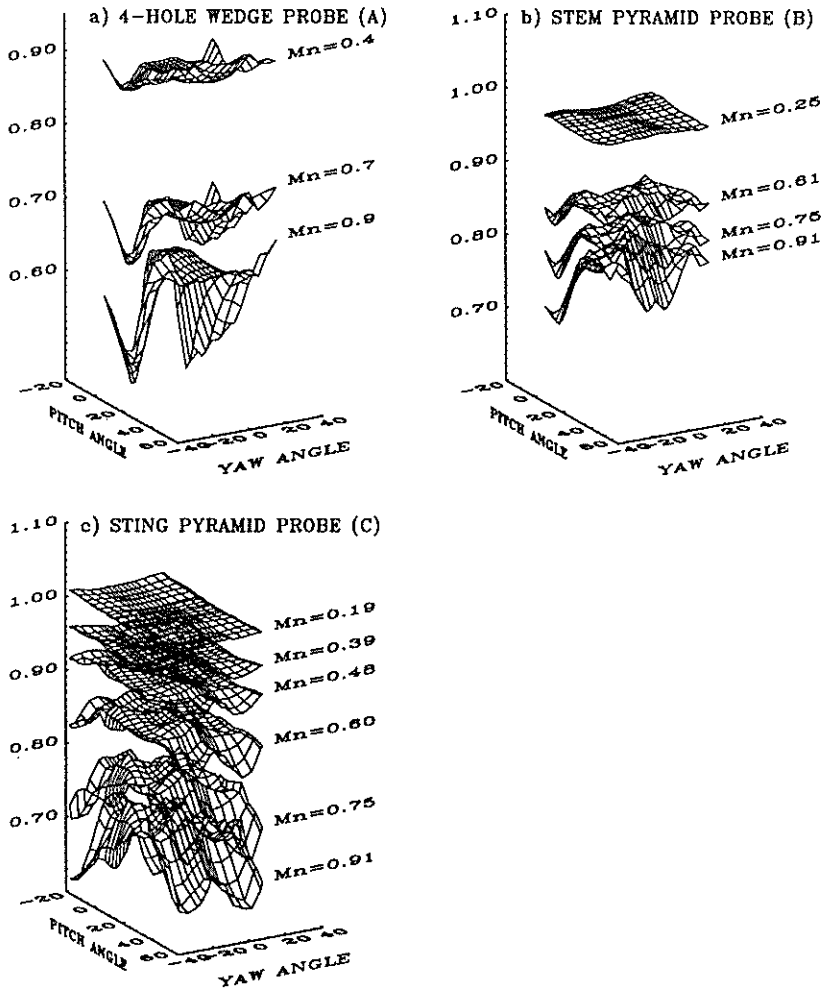

Fig 5: Pressure ratio coefficient behaviour for the 3D pneumatic probes.

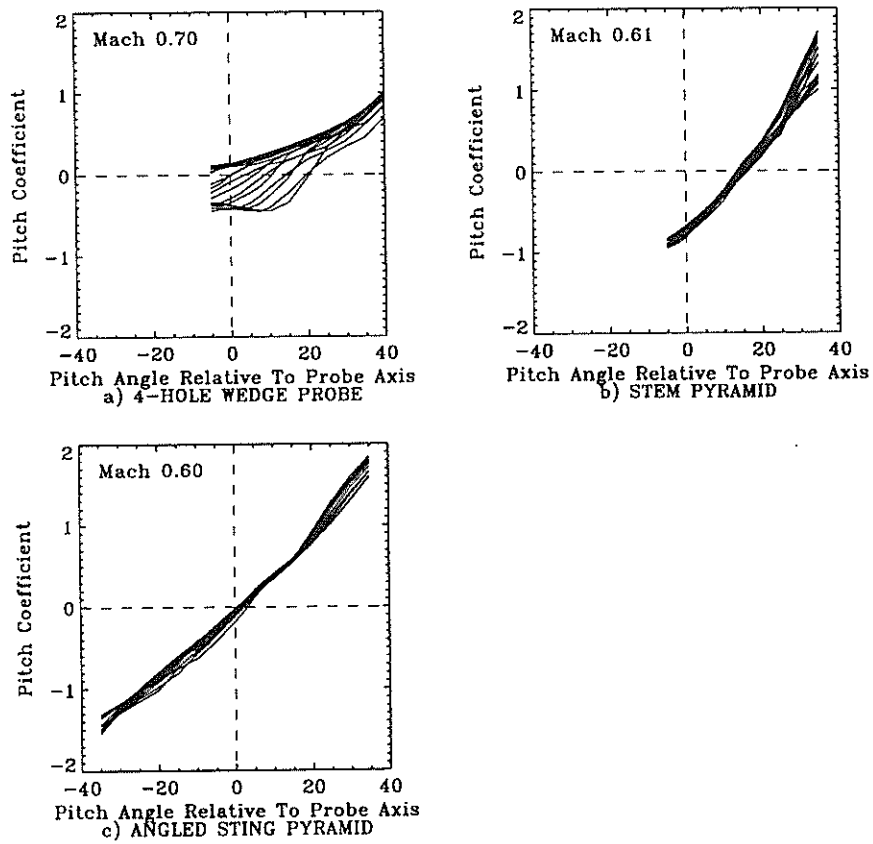

Fig 6: The effect of stem downwash on the 3D pneumatic probes.

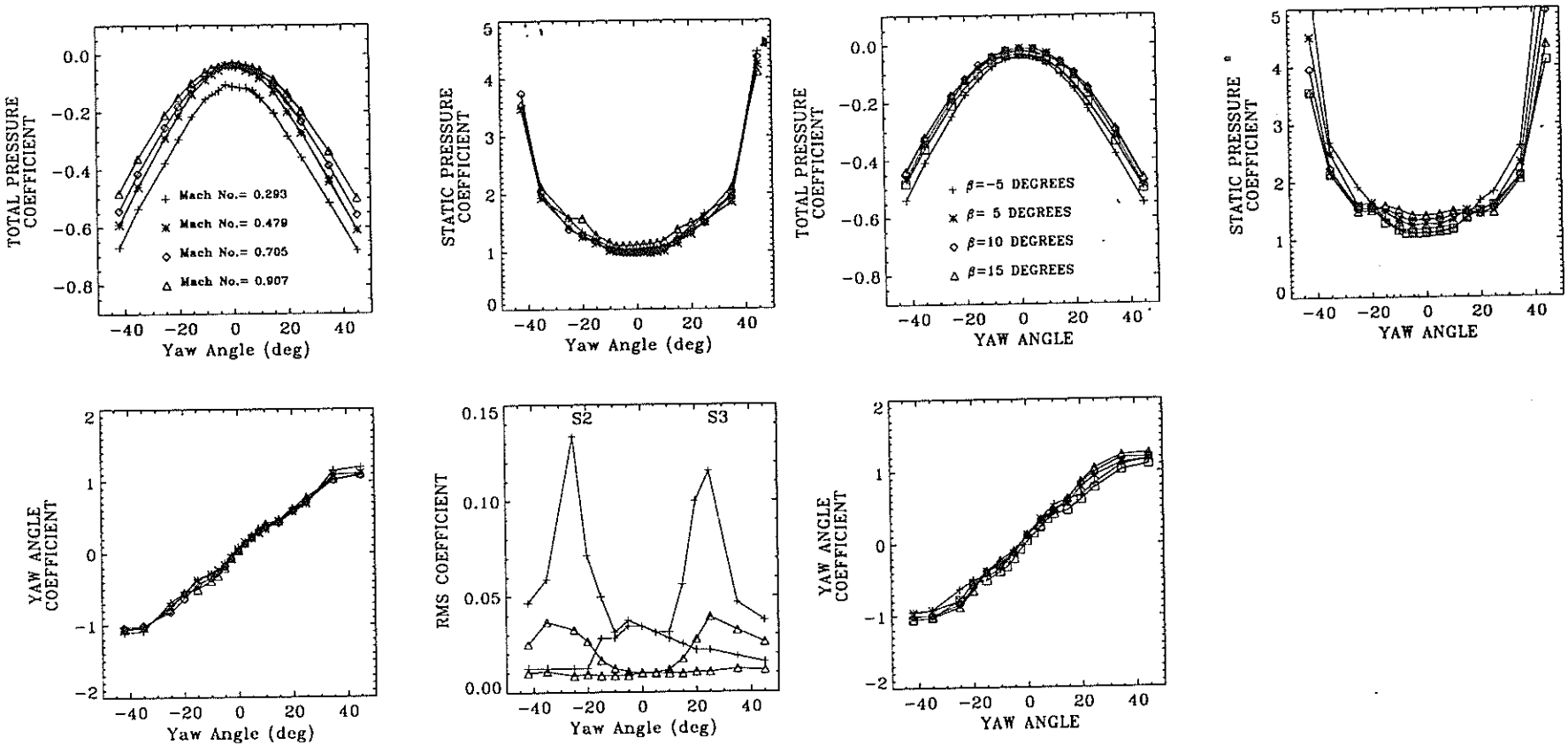

Fig 7: The dynamic yawmeter calibration coefficient behaviour.

Fig 8: The effect of pitch angle on the yawmeter coefficients at Mach 0.9.

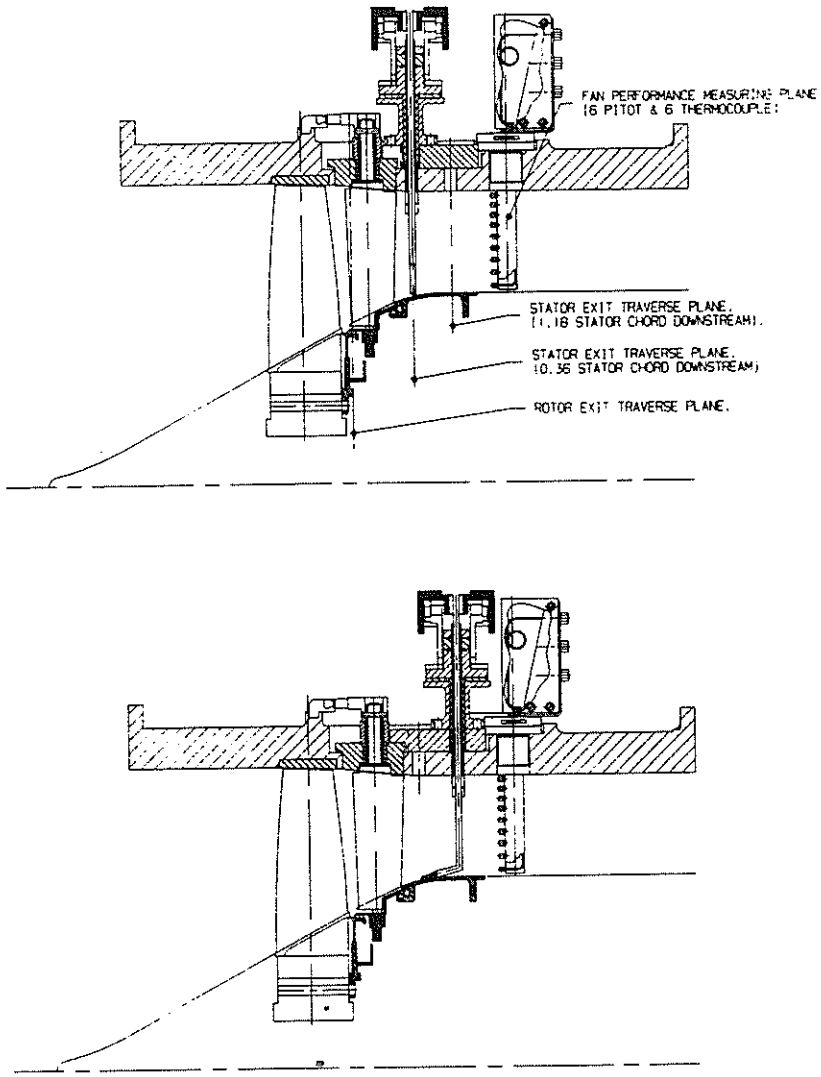

Fig 9: The C148 single stage transonic fan.

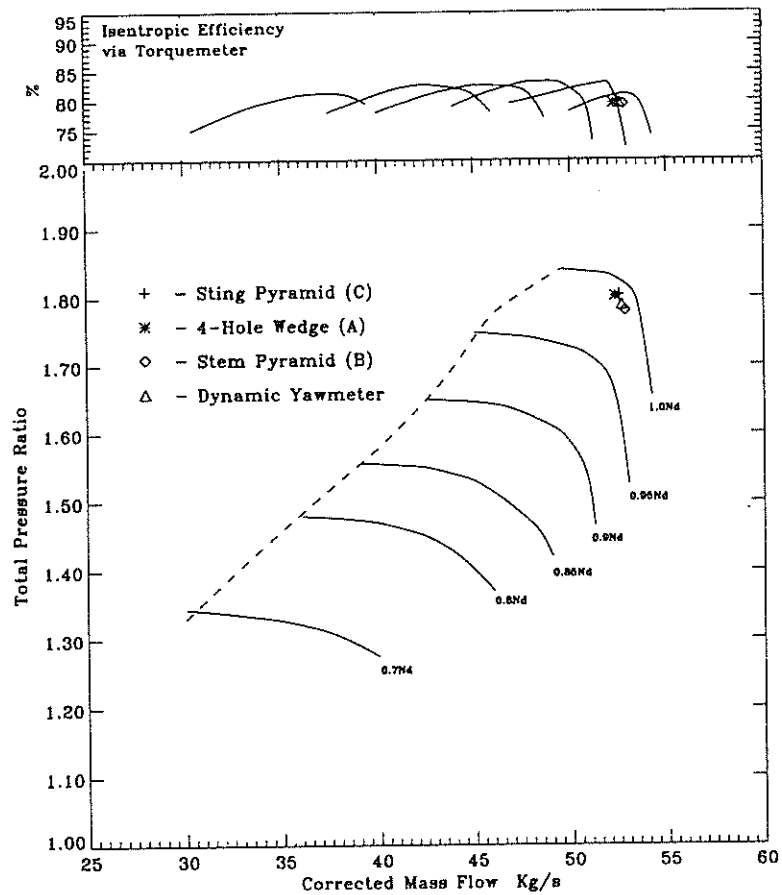

Fig 10: The C148 fan performance characteristic.

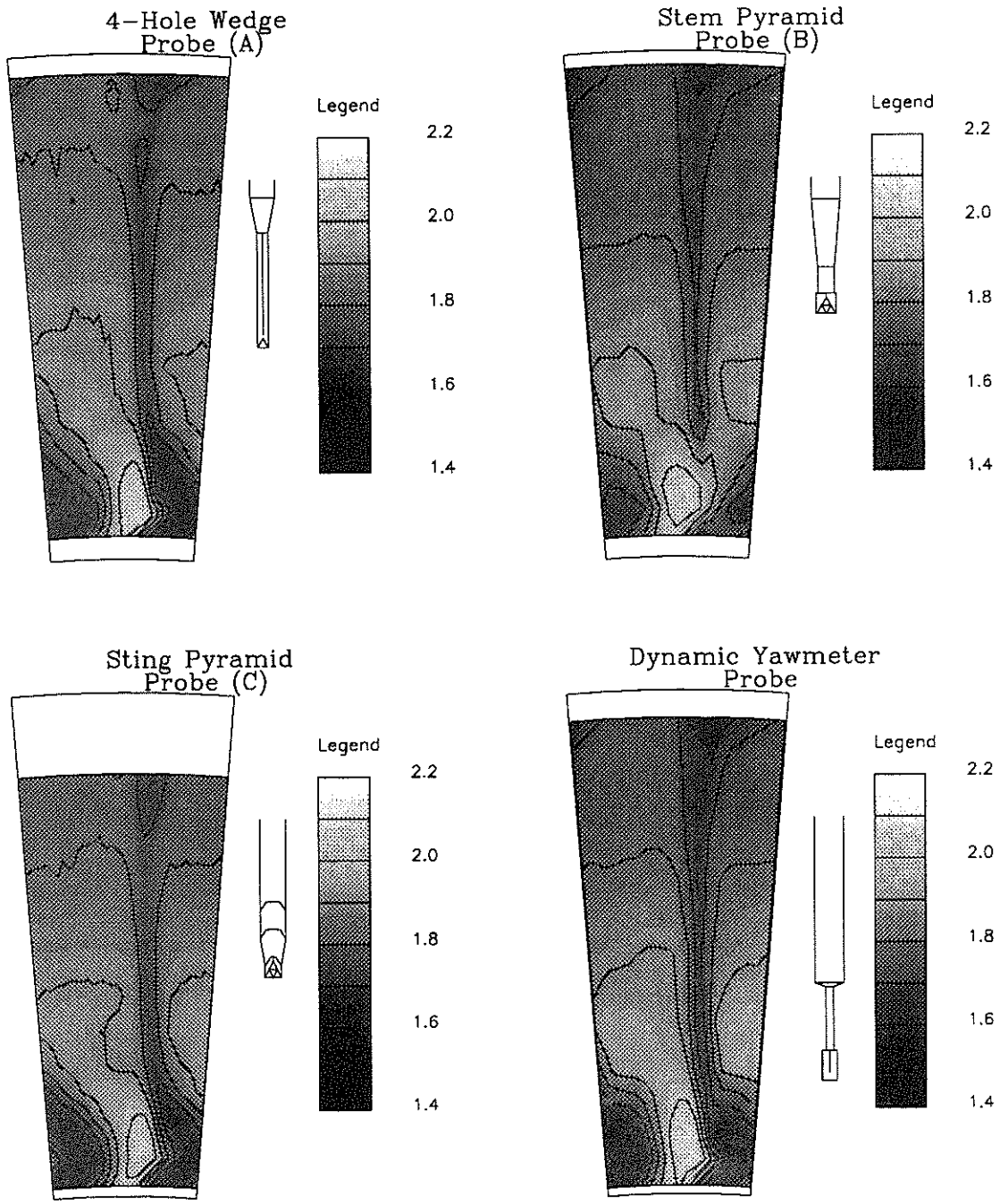

Fig 11: Stagnation pressure ratio measurements taken with the different probes at design speed peak efficiency operation.

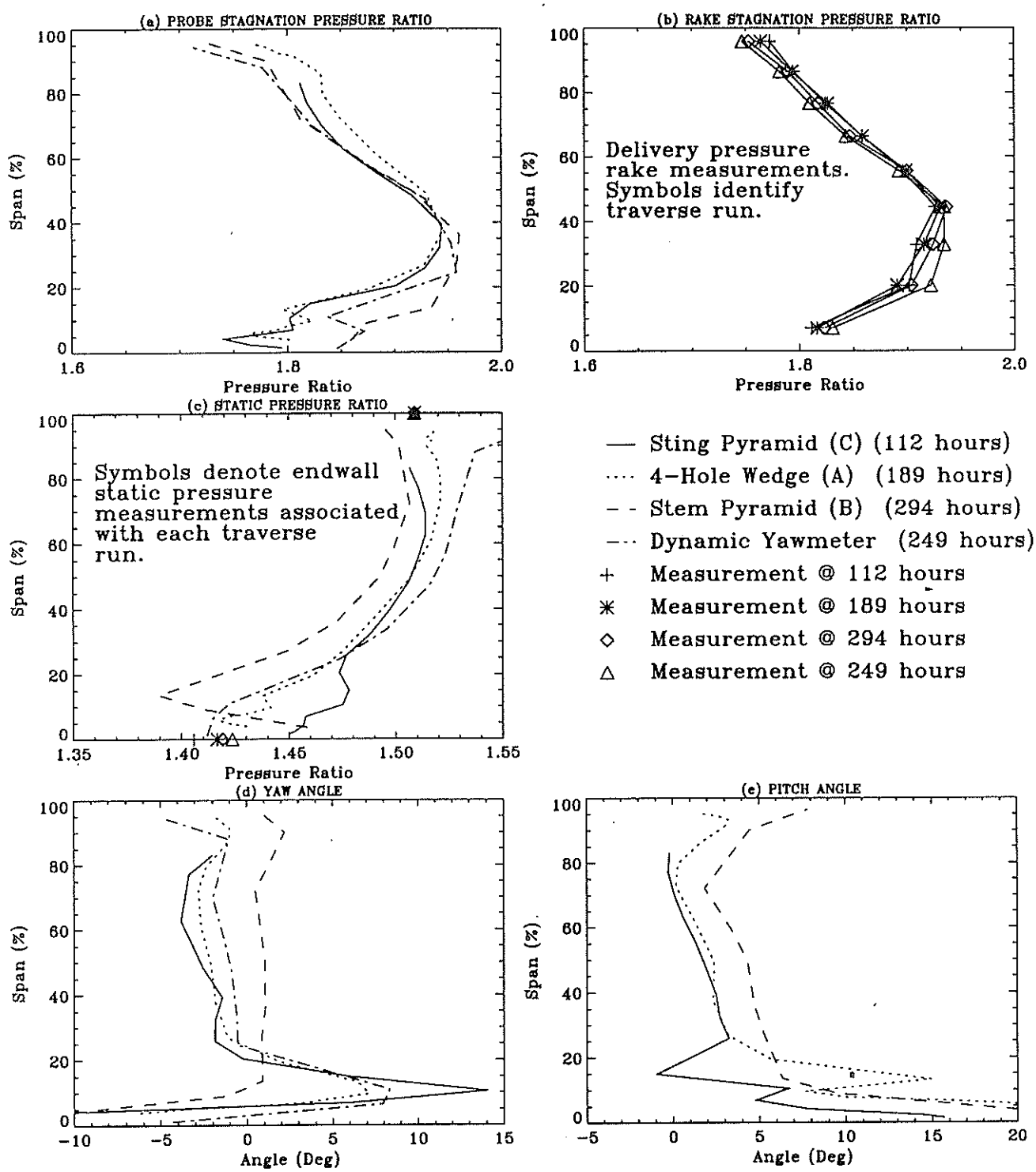

Fig 12: Comparison of the stator exit flowfield measurements taken with the different probes.